Sakarya Üniversitesi Fen Bilimleri Dergisi
Sakarya University Journal of Science

e-ISSN : 2147-835X
Publisher : Sakarya University

Vol. 29, No. 5, 592-601, 2025
DOI: https://doi.org/10.16984/saufenbilder.1704126

Research Article

Flow Patterns Around a Sphere in Terms of Wall Proximity

Ilker Goktepeli[1*], Murat Ispir[1], Muharrem Hilmi Aksoy[1]

[1] Konya Technical University, Faculty of Engineering and Natural Sciences, Department of Mechanical Engineering, Konya, Türkiye, igoktepeli@ktun.edu.tr, mispir@ktun.edu.tr, mhaksoy@ktun.edu.tr, ror.org/02s82rs08
[*] Corresponding Author

ARTICLE INFO

Keywords:
Boundary layer
Gap ratio
Reynolds number
Sphere
Wall proximity

Article History:
Received: 22.05.2025
Revised: 05.09.2025
Accepted: 22.09.2025
Online Available: 21.10.2025

ABSTRACT

Flow over a sphere exhibits three-dimensional phenomena even at lower values of Reynolds number (Re). Nonetheless, three-dimensional flow structures may also be affected by boundary layers on the rough walls. For this reason, the effects of wall proximity are very significant for the present case. Regarding these issues, flow characteristics of a sphere have been examined for several gap ratios from $G^* = 0.01$ to $G^* = 2$ at $Re = 250$. The influence of jet flow between the sphere and the wall has increased by decreasing the gap ratio. Although symmetrical flow patterns have been observed for $G^* = 1$ and $G^* = 2$, this situation is not valid for $G^* \leq 0.5$ in the present study. It is clearly observed in the wake regions for $G^* \leq 0.25$ and the positive cross-stream velocity components become more dominant, especially for $G^* = 0.1$ and $G^* = 0.25$, respectively. The positive spanwise vorticity component becomes more dominant; however, the negative one is more dominant for $G^* \leq 0.1$ in terms of gap ratios. For the case of $G^* \leq 0.05$, the drag coefficients are less than $C_D = 0.47$ and these values are so close to each other. For $G^* = 0.1$, it is around $C_D = 0.5$ for the present problem. By increasing the gap ratios, drag coefficient values also indicated an increasing trend. Moreover, $C_D = 0.579$ has been attained for the case of $G^* = 0.25$ and it is approximately $C_D = 0.68$ for $G^* = 0.5$ as observed. On the other hand, the values of $G^* = 1$ and $G^* = 2$ approached the values of the uniform flow conditions and the effect of the wall proximity by the boundary layer of the bottom surface disappeared.

1. Introduction

Flow characteristics around bluff bodies are important for discussions about aerodynamics. Viscous fluid flow over a sphere could be evaluated as a simplified problem in terms of a prevailing family of immersed bluff bodies owing to its widespread applications [1]. Furthermore, flowing past a sphere indicates three-dimensional phenomena even for lower Reynolds number values [2]. The vortex behavior with instability could show the nature of the resulting flow and large scale shed vortices around these bodies are related to the shear layers separation from the spherical surfaces [3]. Therefore, investigation of flow past a sphere is linked to various engineering applications and the particle transport is considered due to its modelling as a sphere [4]. The flow interference is seen by the vortex shedding and pressure field in the wake region [5].

Regarding previous issues, various studies on the flow around a sphere are significant due to their consideration in engineering cases and this problem has been examined for the effects of several flow parameters. Sweeney and Finlay [6] observed the drag and lift forces of a sphere attached to a wall for boundary layer effect. Tsutsui [7] considered the turbulent boundary layer influence on flow around a sphere Re = 83000. Different height values have been evaluated for the problem. Martinez et al. [8] considered forces of a sphere and a cylinder close to a wall in a boundary layer. Mongruel et al. [9] presented a study on the sphere approach to a

Cite as: I. Goktepeli, M. Ispir, M. H. Aksoy, “Flow patterns around a sphere in terms of wall proximity,” Sakarya University Journal of Science, vol. 29, no. 5, pp. 592-601, 2025. https://doi.org/10.16984/saufenbilder.1704126

wall. Liu and Prosperetti [10] considered the influence of walls on a rotating sphere. Yahiaoui and Feuillebois [11] scrutinized the lift effect on a sphere moving close to a wall in terms of parabolic flow. Dey et al. [12] studied the turbulent wake flows of a sphere on a rough wall. Rodriguez et al. [13] numerically investigated the flow around a sphere. Homann et al. [14] scrutinized the effects of drag and lift fluctuations for a sphere and its boundary layer. Hajimirzaie et al. [15] presented a study for flow around a surface-mounted spherical body in a boundary layer. Chastel and Mongruel [16] observed the flow between a sphere and a textured wall. Zhao et al. [17] examined the vortex structures of a sphere by considering the boundary layer effect at Re = 4170. Experimental study has been presented by van Hout et al. [18] for the sphere wake immersed in a boundary layer. Tee et al. [19] studied the motion of spheres in a turbulent boundary layer. Numerical simulations have been carried out by Yin and Ong [20] for the wake flow of a sphere in a pipe at lower Reynolds number values. Chandel and Das [21] examined the effects of wall proximity on the wake regions of a rotating and translating spheres. Chizfahm et al. [22] numerically studied the flow-induced vibrations of a sphere in terms of free surface proximity. Feng et al. [23] determined the effects of the wall on the flow dynamics for a sphere in motion. Shang et al. [24] simulated the flow characteristics around a sphere on a flat plate for boundary layer. Shepard et al. [25] considered the flow structure for the junction of cylinder-sphere. Li et al. [26] investigated the flow interaction between a sphere and turbulent boundary layer. Kumar et al. [27] examined the wall influence on the sphere wake for the transverse rotation. Considering the previous studies, flow charactistics of a sphere have been examined for different gap ratios.

The purpose of this study is to investigate the impact of gap ratios on the flow dynamics surrounding a sphere at a Reynolds number of 250. As previously highlighted, the flow around a sphere demonstrates three-dimensional characteristics even at lower Reynolds number values. However, the three-dimensional flow patterns could also be influenced by the boundary layers on rough surfaces. It is widely recognized that there are few studies available in open literature regarding the effects of wall proximity. Nevertheless, it is essential to take into account the boundary layer effects for spherical objects in engineering applications.

2. Numerical Method

In the present study, as presented in Figure 1, three-dimensional flow volume has been established for flow around a sphere having a diameter of D = 12.5 mm close to the wall in terms of the different gap ratios ranging for $0.01 \leq G^* = G/D \leq 2$. The dimensions for the flow volume are $-20 \leq x^* = x/D \leq 40$, $-20 \leq y^* = y/D \leq 20$ and $-20 \leq z^* = z/D \leq 20$. The sphere is at $x^* = y^* = z^* = 0$. Aerodynamic flow characteristics have been considered for $Re = U_\infty D \nu^{-1} = 250$ by the kinematic viscosity for air. Uniform velocity has been used at the inlet. For the outlet of the three-dimensional flow volume, pressure outlet has been considered. As implemented for the spherical surfaces, wall boundary condition has been applied for both top and bottom walls.

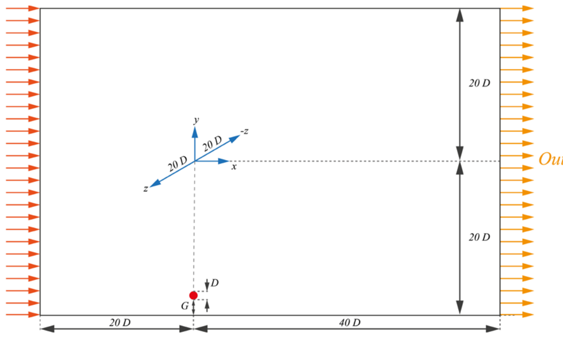

Figure 1. Schematic of the present study

In the current study, ANSYS-Fluent 2021 R1 has been utilized for numerical simulations. The continuity equation has been indicated by Eq. (1). The momentum equations have been presented in Eqs. (2-4).

These equations are valid for three-dimensional, incompressible flow and steady flow conditions. Furthermore, body forces are negligible. These equations have also been given similarly by Mahir [5]. These equations for three-dimensonal case have been derived from two-dimensional ones [28, 29].

$$\frac{\partial u}{\partial x}+\frac{\partial v}{\partial y}+\frac{\partial w}{\partial z}=0 \quad (1)$$

$$u\frac{\partial u}{\partial x}+v\frac{\partial u}{\partial y}+w\frac{\partial u}{\partial z}=-\frac{1}{\rho}\frac{\partial P}{\partial x}+\nu\left(\frac{\partial^2 u}{\partial x^2}+\frac{\partial^2 u}{\partial y^2}+\frac{\partial^2 u}{\partial z^2}\right) \quad (2)$$

$$u\frac{\partial v}{\partial x}+v\frac{\partial v}{\partial y}+w\frac{\partial v}{\partial z}=-\frac{1}{\rho}\frac{\partial P}{\partial y}+\nu\left(\frac{\partial^2 v}{\partial x^2}+\frac{\partial^2 v}{\partial y^2}+\frac{\partial^2 v}{\partial z^2}\right) \quad (3)$$

$$u\frac{\partial w}{\partial x}+v\frac{\partial w}{\partial y}+w\frac{\partial w}{\partial z}=-\frac{1}{\rho}\frac{\partial P}{\partial z}+\nu\left(\frac{\partial^2 w}{\partial x^2}+\frac{\partial^2 w}{\partial y^2}+\frac{\partial^2 w}{\partial z^2}\right) \quad (4)$$

Velocity components have been used in these equations. The variations of the velocity components in respect to three-dimensional coordinates have been taken into account. Pressure, density and kinematic viscosity terms have been included in the equations. For pressure-velocity coupling, the coupled scheme has been used. Gradient, pressure and momentum have been considered for spatial discretization. The convergence has been attained by 10^{-6} for these equations.

The grid structure has been shown for a sample case of G* = 0.01 in Figure 2. For the grid structures, element size has been defined. Inflation has been applied by smooth transition with the growth rate of 1.2 for maximum five layers. For several element sizes, the number of grid elements has been changed.

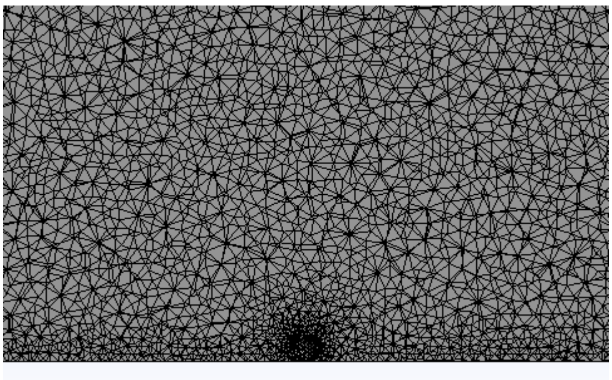

Figure 2. The grid structure

All grid structures have been compared by the drag coefficient of a sphere at Re = 250 for uniform flow conditions. The grid numbers of 1.6×10^6, 2.9×10^6 and 5.3×10^6 have been tested. The following results have been listed in Table 1. The drag coefficients are $C_D = 0.733$ for 1.6×10^6 grid elements, $C_D = 0.734$ for 2.9×10^6 grid elements and $C_D = 0.727$ for 5.3×10^6 grid elements.

Table 1. Drag coefficients with respect to the grid numbers

Grid numbers	C_D
1.6×10^6	0.733
2.9×10^6	0.734
5.3×10^6	0.727

The grid element number of 2.9×10^6 has been chosen for the numerical simulations since the value is in good agreement in the previous results as $C_D = 0.7$ [1], $C_D = 0.702$ [2], $C_D = 0.7$ [3] and $C_D = 0.702$ [4] at Re = 250.

3. Results and Discussion

The present case has been examined by considering the effects of gap ratios on flow patterns around a sphere at Re = 250. In terms of gap ratios, the range of $0.01 \le G^* \le 2$ has been taken into account. The numerical results of pressure distributions, streamwise velocity components, cross-stream velocity components, velocity magnitude values, spanwise vorticity components, vorticity magnitude values and drag coefficient values have been presented with respect to the change of gap ratios. The non-dimensional legends have been given for each situation.

Pressure distributions of $P^* = P\,\rho^{-1}\,(U_\infty)^{-2}$ have been presented from P* = -0.3 to P* = 0.55 as in Figure 3. The highest value has been attained at the upstream of the sphere. This situation is due to the flow stagnation. It is more obvious for the cases of G* = 1 and G* = 2. On the other hand, the values tend to decrease because of decrement in the gap ratios. Moreover, the effective regions indicated shrinkage as the sphere came closer to the bottom wall. Because jet flow effect between the sphere and the wall increased by decreasing the gap ratio. Another influence is the increasing effect of the boundary layer of the bottom wall. Furthermore, flow separations from the upper and the lower surfaces of the sphere have been affected. This observation has been clearly obtained by the minimum pressure zones. The minimum pressure values have been attained in the regions where flow acceleration is seen. The increment of velocity values triggered the pressure drops. It is attributed to the flow separation from the upper and the lower surfaces of the sphere. On the contrary, the decreasing gap ratios caused the disappearance of the lower

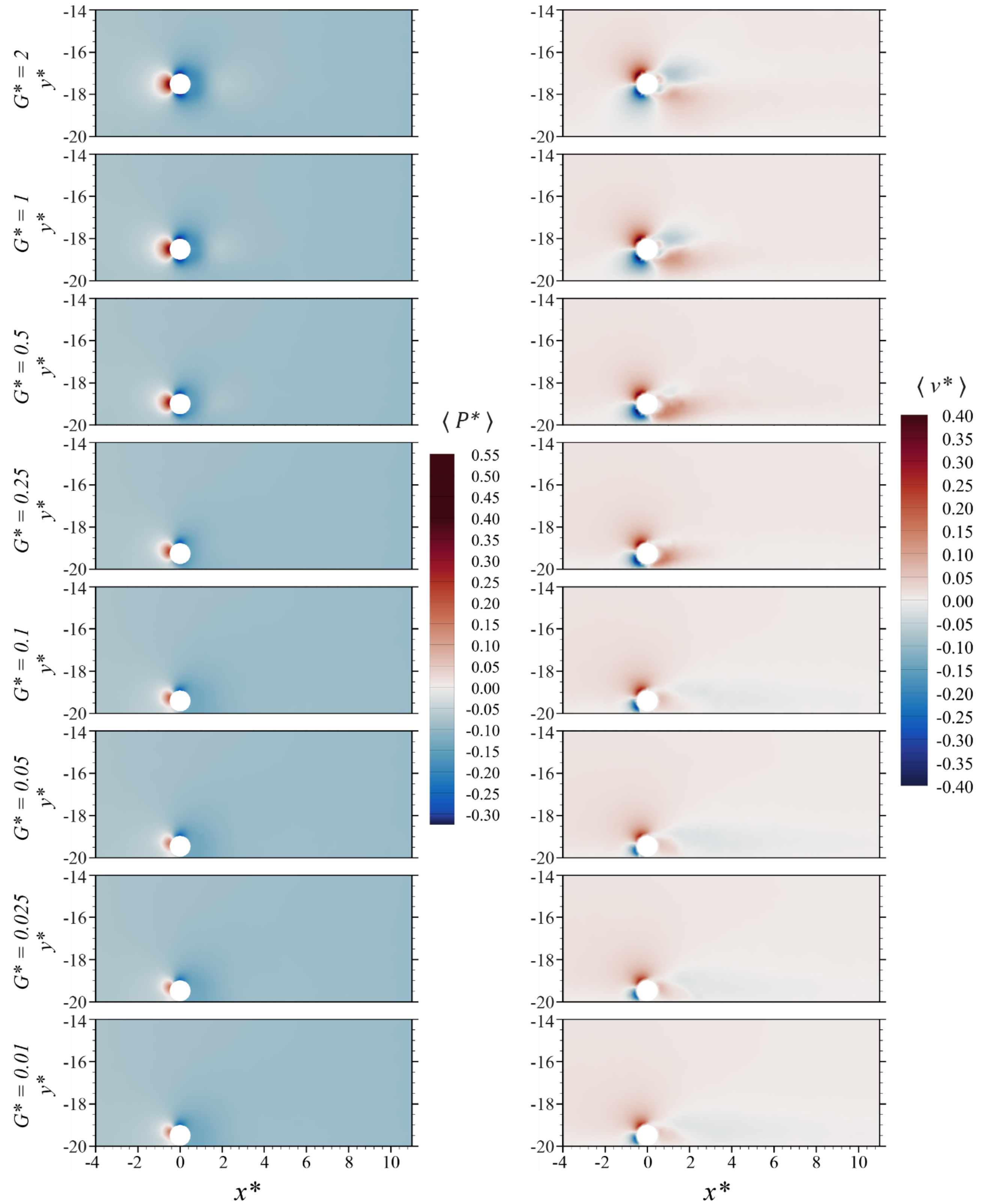

Figure 3. Pressure distributions and cross-stream velocity components with respect to the gap ratios

zones with minimum pressure values. Moreover, the values of the upper regions tended to decrease because of the same reason.

Cross-stream velocity components have been obtained as $v^* = v\,(U_\infty)^{-1}$ for the values ranging from $v^* = -0.4$ to $v^* = 0.4$ as in Figure 3. The peak value has been attained in the upper region of the upstream. On the other hand, the lowest value has been obtained in the lower region of the upstream. Damping of these clusters is valid for the symmetrical axis. For $G^* = 2$, two positive

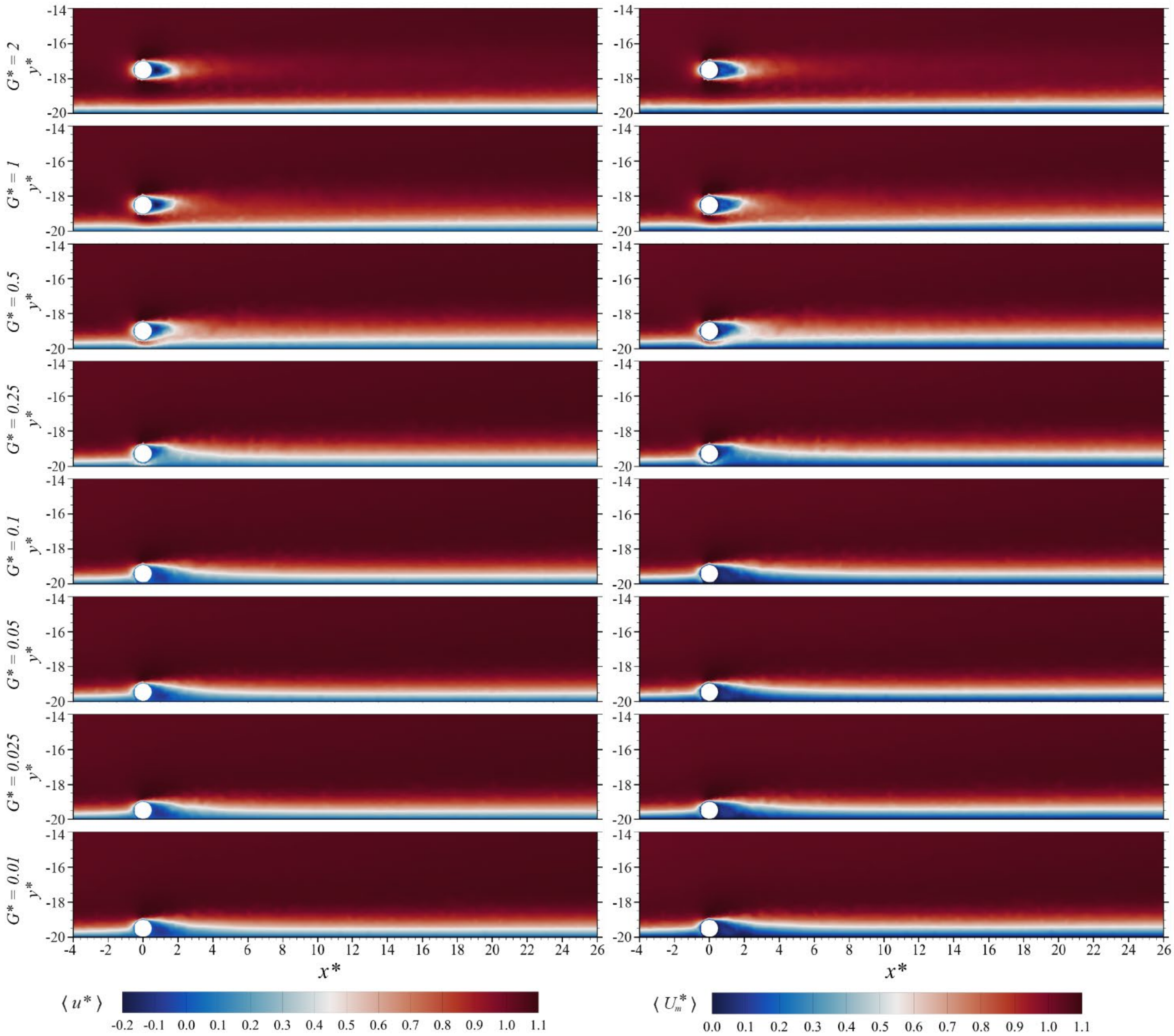

Figure 4. Streamwise velocity components and velocity magnitude values with respect to the gap ratios

and two negative clusters have been observed in the wake region. For these clusters, the positive one and the negative one are smaller and closer to the sphere. Similar situations have also been seen in the case of G* = 1. However, this effect has been diminished by the interaction of the wake flow and the boundary layer of the bottom wall. It is clearly observed in the wake regions for the case of G* ≤ 0.25 and the positive one becomes more dominant especially for the cases of G* = 0.1 and G* = 0.25 as in the graphics. On the contrary, for G* ≤ 0.05, the negative one has been attained as more dominant because of flow separation and jet flow diminishing the positive one.

Streamwise velocity components have been presented as $u^* = u\,(U_\infty)^{-1}$ and given in the range from u* = -0.2 to u* = 1.1 as in Figure 4. The maximum value has been obtained in the regions where no effect of sphere is valid. On the other hand, the minimum value has been attained in the wake regions of the sphere for 0.5 ≤ G* ≤ 2. However, for G* ≤ 0.25, it has been observed by the interaction between the wake flow and the boundary layer of the rough wall. What is more, the size change in the region has been obviously seen because of decrement in the gap ratios. The wake length is nearly 2D for G* = 2 and it is around 1.95D for G* = 1. For G* = 0.5, it is approximately 1.9D due to the beginning of the wall effect. Moreover, symmetrical flow patterns have been observed for G* = 1 and G* = 2. This situation is not valid in the case of G* = 0.5 as in the figure. For this reason, the wake regions have been combined by the boundary layer of the bottom wall. This effect has been clearly observed up to even x* = 12.5 for G* ≤ 0.25 as

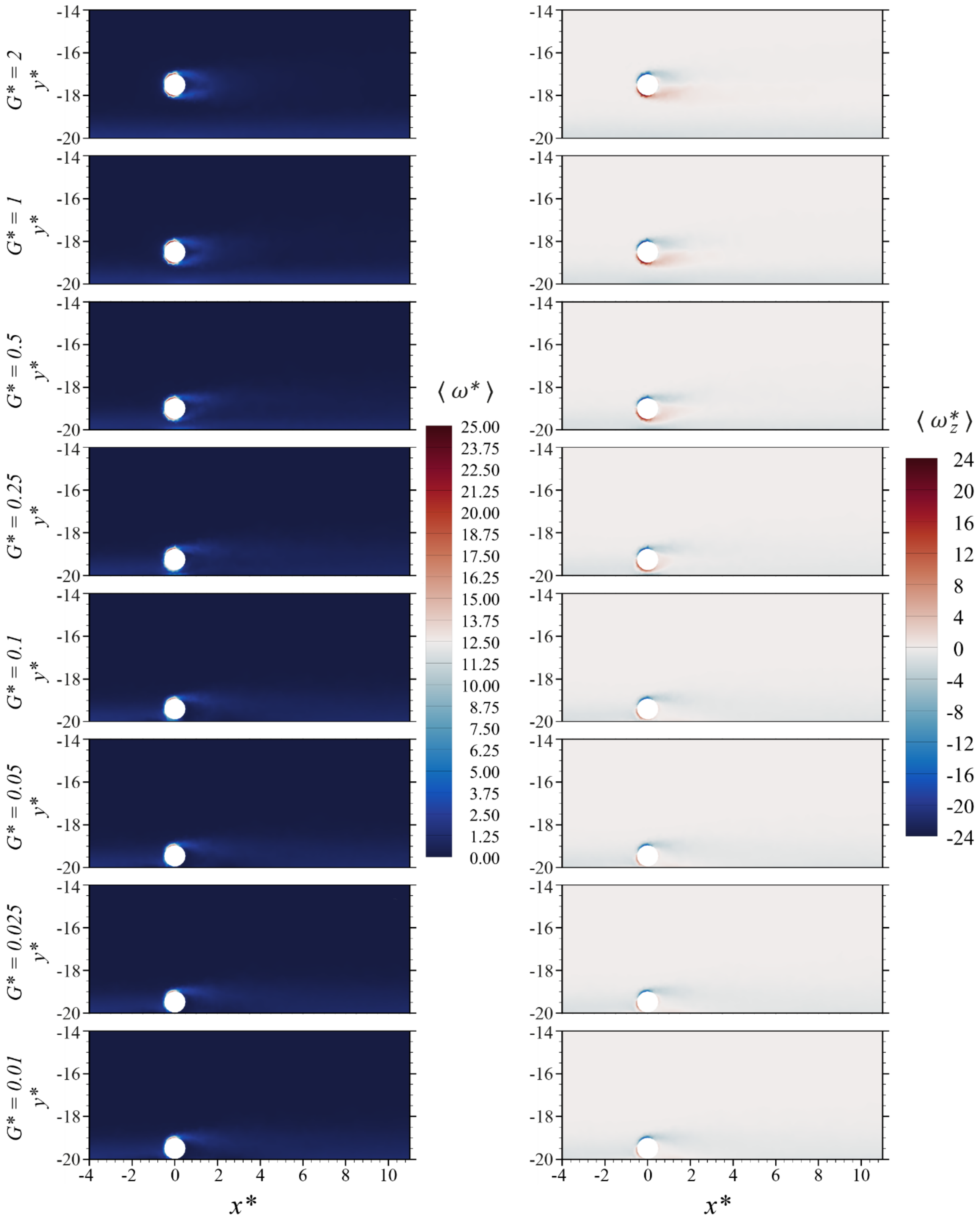

Figure 5. Vorticity magnitude values and spanwise vorticity components with respect to the gap ratios

presented in the contour graphics. On the other hand, these regions have shown shrinkage.

Velocity magnitude values have been attained as $U_m* = U_m (U_\infty)^{-1}$ from $U_m* = 0$ to $U_m* = 1.1$ as in Figure 4. In the zones with no sphere effect, the peak value has been attained. In the wake regions of the sphere for $0.5 \leq G* \leq 2$, the minimum value has been obtained. Nonetheless, it has been seen because of the interaction of the wake flow and the boundary layer of the wall for $G* \leq 0.25$. The size change in the region has also been seen by the decreasing gap ratios. Even though symmetrical flow structures are valid for $G^* = 1$ and $G^* = 2$, it is not observable for $G^* = 0.5$ as in the figure. For this reason, flow patterns have been considerably observed for $G^* = 0.25$ because of the influence triggered by the boundary layer. Based on this deduction, it caused the combination of the wake regions and the boundary layer of the bottom wall. On the contrary, these zones have indicated shrinkage via the decrement of the gap ratios.

Vorticity magnitude values have been presented as $\omega^* = \omega D (U_\infty)^{-1}$ in the range from $\omega^* = 0$ to $\omega^* = 25$ as in Figure 5. The peak value has been obtained by both upper and lower regions of the sphere upstream. On the contrary, the lowest value has been seen in the regions with no vortices. The damping is valid for these zones on the symmetrical axis. Nonetheless, its effect has been diminished by the interaction of the wake flow and the boundary layer of the bottom surface. It is obviously seen for $G^* = 0.25$ as given in the figures. The maximum value one becomes more dominant only in the upper zone of the sphere upstream for the same case. What is more, flow separation and jet flow affected the patterns for the contour graphics. Another influence is the value decrement and the shrinkage for these clusters and it is due to the gap ratio decrement between the sphere and the wall.

Spanwise vorticity components have been given as $\omega_z^* = \omega_z D (U_\infty)^{-1}$ ranging from $\omega_z^* = -24$ to $\omega_z^* = 24$ as in Figure 5. The highest value has been seen in the lower region of the sphere. On the other hand, the minimum value has been observed in the upper region of the body. The damping of positive and negative ones is valid on the symmetrical axis. Nevertheless, this influence has disappeared by the interaction of the wake flow and the wall boundary layer. It is clearly observed for $G^* = 0.25$ and $G^* = 0.5$ as given in the figures. The positive one becomes more dominant as in the contour graphics of the present study. On the other hand, the negative one is more dominant for $G^* \leq 0.1$ because of flow separation and jet flow diminishing the positive one. With respect to the observations, nnother effect is the changes for both value and cluster size. The decreasing gap ratios is the reason for these situations.

In Figure 6, the effects of the gap ratios on the drag coefficient values have been presented. For $G^* \leq 0.05$, the drag coefficients are less than $C_D = 0.47$ and these values are so close to each other as given in the chart. For $G^* = 0.1$, it is around $C_D = 0.5$ for the present problem. For increasing gap ratios, drag coefficient values also increased. Moreover, $C_D = 0.579$ has been attained for the case of $G^* = 0.25$ and it is approximately $C_D = 0.68$ for $G^* = 0.5$ in terms of drag coefficient values. On the other hand, the values of $G^* = 1$ and $G^* = 2$ approached the values of the uniform flow conditions and the effect of the wall proximity by the boundary layer of the bottom surface disappeared.

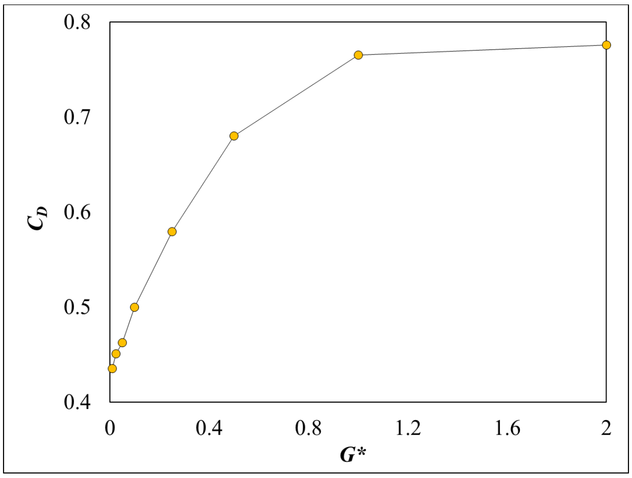

Figure 6. Drag coefficients with respect to the gap ratios

The drag reduction near the wall could be explained by decomposing it into pressure drag and viscous drag contributions. Drag due to pressure dominates, however, viscous effects are still inevasible for the current Reynolds number. When a sphere is close to a wall, the wake symmetry has been broken. The situation led to the wake shrinkage. It is linked to the drag reduction [30]. Moreover, pressure difference between the upstream and the downstream has been reduced. Decrement of drag due to pressure has been seen and it indicated lower drag coefficient near the wall. The drag owing to viscous effects may increase slightly owing to the wall-induced shear; however, it is still lower than drag reduction due to pressure. For lower gap ratios, the jet effect lost its ability to penetrate and deflect the flow mechanism, owing to the attenuation triggered by the significant influence of the near-wall boundary layer and the proximity to the wall. It also included the combination of reduced jet momentum relative to boundary layer shear, suppression of vortex formation and viscous effects near the wall.

4. Conclusions

Aerodynamic flow characteristics of a sphere have been examined for different gap ratios from G* = 0.01 to G* = 2 in the present study. Numerical results for pressure distributions, streamwise and cross-stream velocity components, velocity magnitude values, spanwise vorticity components, vorticity magnitude values and drag coefficients have been presented at Reynolds number of Re = 250. Gap ratios affected flow structures around the sphere. A maximum static pressure occurs at the upstream stagnation point. The effect of the jet flow has increased by decreasing the gap ratio. Another influence is the increasing effect of the boundary layer on the bottom wall. Although symmetrical flow patterns have been observed for G* = 1 and G* = 2 by the streamwise velocity values, this situation is not valid by the case of G* = 0.5 in this study. It is clearly observed in the wake regions for G* ≤ 0.25 and the positive cross-stream component value becomes more dominant especially for the cases of G* = 0.1 and G* = 0.25 in the current study. On the contrary, for G* ≤ 0.05, the negative one has been attained as more dominant because of flow separation and jet flow diminishing the positive one. The negative spanwise vorticity component value is more dominant for G* ≤ 0.1 as observed. For G* ≤ 0.05, the drag coefficients are less than C_D = 0.47 and these values are so close to each other. For G* = 0.1, it is around C_D = 0.5 for the present study. By increasing gap ratios between the sphere and the wall, drag coefficient values also increased. What is more, C_D = 0.579 has been attained for G* = 0.25 and it is approximately C_D = 0.68 for G* = 0.5, respectively. On the other hand, the values of G* = 1 and G* = 2 approached the values which are valid for the uniform flow conditions.

Article Information Form

Acknowledgments
As a second author, Mr. Ispir expresses his gratitude to the Scientific and Technological Research Council of Türkiye (TÜBİTAK) for a doctoral scholarship in terms of the 2211-A program.

Funding
Authors have not received any financial support for the research, authorship or publication of this study.

Authors' Contribution
IG: Conceptualization, Methodology, Software, Validation, Investigation, Resources, Writing-Original Draft, Writing-Review & Editing
MI: Software, Resources, Data Curation, Writing-Review & Editing, Visualization
MHA: Software, Writing-Review & Editing

The Declaration of Conflict of Interest
No conflict of interest or common interest has been declared by authors.

Artificial Intelligence Statement
No artificial intelligence tool has been used while writing this article.

References

[1] T. Johnson, V. Patel, “Flow past a sphere up to a Reynolds number of 300,” Journal of Fluid Mechanics, vol. 378, pp. 19-70, 1999.

[2] D. Kim, “Laminar flow past a sphere rotating in the transverse direction,” Journal of Mechanical Science and Technology, vol. 23, pp. 578-589, 2009.

[3] G. S. Constantinescu, K. D. Squires, “LES and DES investigations of turbulent flow over a sphere at Re= 10,000,” Flow, Turbulence and Combustion, vol. 70, pp. 267-298, 2003.

[4] D. Kim, H. Choi, "Laminar flow past a sphere rotating in the streamwise direction," Journal of Fluid Mechanics, vol. 461, pp. 365-386, 2002.

[5] N. Mahir, "Three-dimensional flow around a square cylinder near a wall," Ocean Engineering, vol. 36, no. 5, pp. 357-367, 2009.

[6] L. Sweeney, W. Finlay, "Lift and drag forces on a sphere attached to a wall in a Blasius boundary layer," Journal of Aerosol Science, vol. 38, no. 1, pp. 131-135, 2007.

[7] T. Tsutsui, "Flow around a sphere in a plane turbulent boundary layer," Journal of Wind Engineering and Industrial Aerodynamics, vol. 96, no. 6-7, pp. 779-792, 2008.

[8] R. Martinez, L. Sweeney, W. Finlay, "Aerodynamic forces and moment on a sphere or cylinder attached to a wall in a Blasius boundary layer," Engineering Applications of Computational Fluid Mechanics, vol. 3, no. 3, pp. 289-295, 2009.

[9] A. Mongruel, C. Lamriben, S. Yahiaoui, F. Feuillebois, "The approach of a sphere to a wall at finite Reynolds number," Journal of Fluid Mechanics, vol. 661, pp. 229-238, 2010.

[10] Q. Liu, A. Prosperetti, "Wall effects on a rotating sphere," Journal of Fluid Mechanics, vol. 657, pp. 1-21, 2010.

[11] S. Yahiaoui, F. Feuillebois, "Lift on a sphere moving near a wall in a parabolic flow," Journal of Fluid Mechanics, vol. 662, pp. 447-474, 2010.

[12] S. Dey, S. Sarkar, S. K. Bose, S. Tait, O. Castro-Orgaz, "Wall-wake flows downstream of a sphere placed on a plane rough wall," Journal of Hydraulic Engineering, vol. 137, no. 10, pp. 1173-1189, 2011.

[13] I. Rodriguez, R. Borell, O. Lehmkuhl, C. D. P. Segarra, A. Oliva, "Direct numerical simulation of the flow over a sphere at Re= 3700," Journal of Fluid Mechanics, vol. 679, pp. 263-287, 2011.

[14] H. Homann, J. Bec, R. Grauer, "Effect of turbulent fluctuations on the drag and lift forces on a towed sphere and its boundary layer," Journal of Fluid Mechanics, vol. 721, pp. 155-179, 2013.

[15] S. M. Hajimirzaie, A. G. Tsakiris, J. H. Buchholz, A. N. Papanicolaou, "Flow characteristics around a wall-mounted spherical obstacle in a thin boundary layer," Experiments in Fluids, vol. 55, pp. 1-14, 2014.

[16] T. Chastel, A. Mongruel, "Squeeze flow between a sphere and a textured wall," Physics of Fluids, vol. 28, no. 2, p. 023301, 2016.

[17] H. Zhao, X. Liu, D. Li, A. Wei, K. Luo, J. Fan, "Vortex dynamics of a sphere wake in proximity to a wall," International Journal of Multiphase Flow, vol. 79, pp. 88-106, 2016.

[18] R. van Hout, J. Eisma, G. E. Elsinga, J. Westerweel, "Experimental study of the flow in the wake of a stationary sphere immersed in a turbulent boundary layer," Physical Review Fluids, vol. 3, no. 2, p. 024601, 2018.

[19] Y. H. Tee, D. C. Barros, E. K. Longmire, "Motion of finite-size spheres released in a turbulent boundary layer," International Journal of Multiphase Flow, vol. 133, p. 103462, 2020.

[20] G. Yin, M. C. Ong, "On the wake flow behind a sphere in a pipe flow at low Reynolds numbers," Physics of Fluids, vol. 32, no. 10, p. 103605, 2020.

[21] A. Chandel, S. Das, "Effect of wall proximity on the wake of a rotating and translating sphere," Acta Mechanica, vol. 232, pp. 4833-4846, 2021.

[22] A. Chizfahm, V. Joshi, R. Jaiman, "Transverse flow-induced vibrations of a sphere in the proximity of a free surface: A numerical study," Journal of Fluids and Structures, vol. 101, p. 103224, 2021.

[23] Z. G. Feng, J. Gatewood, E. E. Michaelides, "Wall effects on the flow dynamics of a rigid sphere in motion," Journal of Fluids Engineering, vol. 143, no. 8, p. 081106, 2021.

[24] W. Shang, H. Zhao, D. Li, K. Luo, J. Fan, "Direct numerical simulation of the flow around a sphere immersed in a flat-plate turbulent boundary layer," Physics of Fluids, vol. 33, no. 11, p. 115106, 2021.

[25] T. G. Shepard, D. Law, R. K. Menon, K. Ordahl, A. Gutenberg, "Interference drag and flow structure around cylinder-sphere junction," Ocean Engineering, vol. 234, p. 109276, 2021.

[26] D. Li, K. Luo, H. Zhao, W. Shang, J. Fan, "Interaction between a stationary sphere and turbulent flow in a boundary layer," Physics of Fluids, vol. 34, no. 8, p. 085138, 2022.

[27] A. Kumar, S. Das, S. Tiwari, "Wall effect on the wake characteristics of a transversely rotating sphere," Physics of Fluids, vol. 36, no. 1, p. 013611, 2024.

[28] N. Mahir, Z. Altac, "Numerical investigation of convective heat transfer in unsteady flow past two cylinders in tandem arrangements," International Journal of Heat and Fluid Flow, vol. 29, no. 5, pp. 1309-1318, 2008.

[29] I. Goktepeli, "Examination of wake characteristics for tandem circular cylinders via Computational Fluid Dynamics," Journal of Advanced Research in Natural and Applied Sciences, vol. 11, no. 1, pp. 1-11, 2025.

[30] I. Goktepeli, M. Ispir, M H. Aksoy, "Experimental flow control around circular cylinders with porous media coatings," Acta Mechanica, pp. 1-17, 2025.